HYDROLOGICAL PROCESSES
Hydrol. Process. **28**, 5093–5104 (2014)
Published online 28 August 2013 in Wiley Online Library
(wileyonlinelibrary.com) DOI: 10.1002/hyp.9995

Energy flux partitioning and evapotranspiration in a sub-alpine spruce forest ecosystem

Zhu Gaofeng,[1]* Lu Ling,[2] Su Yonghong,[2] Wang Xufeng,[3] Cui Xia,[1] Ma Jinzhu,[1] He Jianhua,[1] Zhang Kun[1] and Li Changbin[1]

[1] *Key Laboratory of Western China's Environmental Systems (Ministry of Education), Collaborative Innovation Centre for Arid Environments and Climate Change, Lanzhou University, Lanzhou, China*
[2] *Division of Hydrology Water–Land Research in Cold and Arid Regions, Cold and Arid Regions Environmental and Engineering Research Institute, CAS, Lanzhou, China*
[3] *Laboratory of Remote Sensing and Geospatial Science, Cold and Arid Regions Environmental and Engineering Research Institute, CAS, Lanzhou, China*

Abstract:

In this study, we examined the year 2011 characteristics of energy flux partitioning and evapotranspiration of a sub-alpine spruce forest underlain by permafrost on the Qinghai–Tibet Plateau (QPT). Energy balance closure on a half-hourly basis was $H + \lambda E = 0.81 \times (R_n - G - S) + 3.48$ (W m^{-2}) ($r^2 = 0.83$, $n = 14938$), where H, λE, R_n, G and S are the sensible heat, latent heat, net radiation, soil heat and air-column heat storage fluxes, respectively. Maximum H was higher than maximum λE, and H dominated the energy budget at midday during the whole year, even in summer time. However, the rainfall events significantly affected energy flux partitioning and evapotranspiration. The mean value of evaporative fraction ($\Lambda = \lambda E/(\lambda E + H)$) during the growth period on zero precipitation days and non-zero precipitation days was 0.40 and 0.61, respectively. The mean daily evapotranspiration of this sub-alpine forest during summer time was 2.56 mm day^{-1}. The annual evapotranspiration and sublimation was 417 ± 8 mm year^{-1}, which was very similar to the annual precipitation of 428 mm. Sublimation accounted for 7.1% (30 ± 2 mm year^{-1}) of annual evapotranspiration and sublimation, indicating that the sublimation is not negligible in the annual water balance in sub-alpine forests on the QPT. The low values of the Priestley–Taylor coefficient (α) and the very low value of the decoupling coefficient (Ω) during most of the growing season suggested low soil water content and conservative water loss in this sub-alpine forest. Copyright © 2013 John Wiley & Sons, Ltd.

Supporting information may be found in the online version of this article.

KEY WORDS energy flux partitioning; evapotranspiration; Qinghai spruce; permafrost; Qinghai–Tibet plateau; sublimation; decoupling coefficient

Received 24 April 2013; Accepted 31 July 2013

INTRODUCTION

The solar radiation absorbed at the surface plays a major role in climatic change. Compared with cropland, grassland and bare soil, forests often have a lower surface albedo and so absorb more solar radiation (Baldocchi and Vogel, 1995; Betts, 2000). The partitioning of the available energy to ecosystem latent (λE) and sensible (H) heat fluxes plays a critical role in atmospheric boundary layer (ABL) dynamics and, hence, directly influences local, regional and even global climate (Wilson *et al.*, 2002a, b). On the other hand, changes in local environmental conditions may affect a variety of physical and physiological processes in plant canopies and finally alter the mass and energy exchange between the surface and atmosphere, forming a direct link to global climate (Wilson and Baldocchi, 2000). Therefore, comprehensive knowledge about the characteristics of the energy partitioning in different forest types at various environmental conditions is important for examining complex interactions between the terrestrial biosphere and atmosphere, water circulation and global climate change (Brubaker and Entekhabi, 1996; Raupach, 1998).

The Qinghai–Tibet Plateau (QTP), known as the 'third pole of the earth', is the only region in the world where the permafrost is present in mid-latitudes and is regarded as one of the most sensitive regions to global changes (Zheng, 1996; Liu and Chen, 2000; IPCC, 2007). Forests cover a wide range of ecological habitats on the QTP and are the highest in the world. Qinghai spruce (Picea crassifolia) is an endemic widespread tree species on northeastern QTP from 2300–3300 m altitude and is

*Correspondence to: Zhu Gaofeng, Key Laboratory of Western China's Environmental Systems (Ministry of Education), Lanzhou University, Tianshui Road 222, Lanzhou, Gansu Province, China, 730000.
E-mail: zhugf@lzu.edu.cn

usually associated with the presence of permafrost. This sub-alpine forest plays a very important role in preventing soil erosion and loss, in regulating climate, and in retaining ecological stabilities of many inland river systems, lake reservoirs and desert oases in northwest China (Zhu *et al*., 2007, 2008; Bourque and Mir, 2012). In recent decades, the eddy covariance (EC) technique has been widely used to measure the exchanges of energy, water and carbon dioxide between the biosphere and atmosphere (Baldocchi *et al*., 2001). For examples, Gu *et al*. (2005) and Yao *et al*. (2011) reported the energy partitioning for the alpine meadow ecosystems on the QTP and found that H was higher than λE in winter and spring, but was lower than λE in summer and autumn. However, the characteristics of the energy flux partitioning and evapotranspiration of the sub-alpine forest ecosystem is still unclear. Also, many single-site studies have been conducted in forest ecosystems such as tropical forests (e.g. Kumagai *et al*., 2005; Fisher *et al*., 2008; Tanaka *et al*., 2008; Giambelluca *et al*., 2009; Kume *et al*., 2011), temperate forests (e.g. Wilson and Baldocchi, 2000; Gu *et al*., 2006; Kosugi *et al*., 2007; Wu *et al*., 2007; Kochendorfer *et al*., 2011; Wu *et al*., 2012) and boreal forests (e.g. Baldocchi and Vogel, 1996; Arain *et al*., 2003; Humphreys *et al*., 2003; McCaughey *et al*., 2006; Pejam *et al*., 2006; Ohta *et al*., 2008; Jassal *et al*., 2009; Sánchez *et al*., 2010; Iwata *et al*., 2012; Nakai *et al*., 2013). Among them, very few studies have dealt with evapotranspiration from forests underlain by permafrost with the exceptions of Iwata *et al*. (2012) and Nakai *et al*. (2013). In addition, the contribution of sublimation to the annual total water vapour flux in many ecosystems is still unclear and need to be further investigated (Nakai *et al*., 2013).

Based on the year-round observation of energy components and water vapour fluxes from the permafrost Qinghai spruce forest on the QTP in 2011, the objectives of the present study were to: (1) characterize the patterns of diurnal and seasonal variation in energy flux partitioning and evapotranspiration in a sub-alpine forest; (2) identify the contribution of sublimation to the annual total water vapour flux from the sub-alpine forest; and (3) determine the diagnostic parameters characterizing energy flux partitioning and evapotranspiration.

MATERIALS AND METHODS

Site description

The study area is located at Guantan freeze/thaw observation station (38°32′1″N, 100°15′1″E) on the northeastern QTP, China. This station was set up and instrumented in June 2008 as part of the Watershed Allied Telemetry Experimental Research project (see details in Li *et al*., 2009). The site was surrounded by continuous mountains with elevations ranging from 2700–3400 m a.s.l. The prevailing daytime wind directions at this site were north and northeast during different seasons. The forest fetch along the prevailing wind directions is about 970 m (see details in Appendix A). According to the meteorological observation at a nearby meteorological station (Xishui experimental station; 38°24′N, 100°17′E; 2800 m a.s.l.) from 1994–2010, the mean annual precipitation and air temperature at this site are 435 mm and 0.5 °C, respectively (Liu *et al*., 2010). The overstory tree species at the study site is Qinghai spruce (*P. crassifolia*) with the forest floor nearly covered by a layer of moss with a depth of 10 cm. The moss layer may insulate mineral soil from weather extremes such as high temperatures in summer and maintain the high permafrost table (Nakai *et al*., 2013). The soil is classified as mountain gray-cinnamon forest soil with an average thickness of about 120 cm. The topsoil (0–40 cm) is the humus layer and high in soil organic matter (ca. 17 g kg^{-1}), whereas the subsoil (40–120 cm) was the argillic layer, which was mainly consisted of fine sand (see details in Appendix A). The root mass (ca. 64%) was mainly distributed in 20–40 cm soil layers. A tree survey of this forest was conducted in September 2009. The characteristics of the trees including tree height, canopy height, diameter at breast height (DBH) and crown diameter were measured in a 100 m × 100 m plot containing 1186 trees with DBH > 5.0 cm. The mean canopy height of these 1186 trees was 10.5 m ranging from 0.6–11.6 m.

Energy balance measurements

The surface energy balance is described by the equation

$$R_n = H + \lambda E + G + S \quad (1)$$

All components in Equation (1) are expressed as energy fluxes in W m^{-2}. R_n is the net radiation, H is the sensible heat flux, λE is the latent heat flux, G is the soil heat flux, and S is the air-column storage heat flux. Net radiation was measured at a height of 20 m above the soil with a net radiometer (CNR-1; Kipp & Zonen, Delft, Netherlands), which consisted of four radiometers to measure the incoming and reflected short-wave radiation (S_d, S_u), and incoming and outgoing long-wave radiation (L_d, L_u).

The sensible and latent heat fluxes were measured using the EC system (e.g. Webb *et al*., 1980; Baldocchi *et al*., 2000), which was installed on a relatively flat terrain in the mountainside with a topographic slope of 3° (see details in Appendix A). The EC measurements included a three-dimensional sonic anemometer (CSAT3, Campbell Scientific Inc., UT, USA) to measure vertical wind speed and air temperature fluctuations, and an open-path infrared gas analyser (Li-7500, LI-COR Inc., USA) to measure the water vapour density and carbon dioxide fluctuations. The anemometer and open-path gas analyser were installed at the height of 20.25 m above the ground.

The EC data were sampled at a frequency of 10 Hz, and the turbulent fluxes were continuously recorded by a data logger (CR5000, Campbell Scientific Inc.). The calibration for the gas analyser was made every year at the beginning of the growing season using a span gas of known CO_2 concentration and a dew point generator (LI-COR Inc., 2000). Based on the footprint analysis for unstable stratification presented by Hsieh *et al.* (2000), the peak for the flux footprint is located at approximately 40 m upwind. The 90% flux fetch was at the distance of about 410 m upwind in the unstable condition (Appendix A). Thus, the measured fluxes were primarily contributed by the forest.

Soil heat flux (G) was determined using the equation described by Oliphant *et al.* (2004):

$$G = G_z + \rho_s C_s \int_0^z \frac{\partial T_s}{\partial t} dz \quad (2)$$

where G_z is the heat flux measured at depth z (5 cm at our site), ρ_s is the soil density (kg m^{-3}), C_s is the specific heat of soil (J kg^{-1} K^{-1}), T_s is the soil temperature (K), and t is the time (s). Soil heat flux was measured using three soil heat transducers (HFT01; Campbell Scientific Inc.), and soil temperature above the transducers (at 3 cm below the surface) were measured by thermocouple thermometry (109; Campbell Scientific Inc.). The soil thermal capacity can be approximately expressed as

$$\rho_s C_s = \rho_{dry} C_{dry} + \rho_w C_w \theta \quad (3)$$

where ρ_{dry} is the dry soil density (kg m^{-3}), C_{dry} is the specific heat of the soil minerals (J kg^{-1} K^{-1}), ρ_w is the water density (kg m^{-3}), C_w is the specific heat of water (J kg^{-1} K^{-1}), and θ is the volumetric water content (%), which was measured with TDR sensors (CS616; Campbell Scientific Inc.) at 3 cm below the surface.

Heat storage terms (S) were estimated as (Oliphant *et al.*, 2004):

$$S = S_v + S_a + S_\lambda \quad (4)$$

where S_v is the change in heat storage associated with wood biomass, which was neglected in this study due to its low contribution to total heat storage (<5%) (Blanken *et al.*, 1997; Oliphant *et al.*, 2004). S_a and S_λ are the changes in heat storage forced by changes in canopy air temperature and specific humidity, respectively, and they are calculated as

$$S_a = \rho C_p \int_0^{z_r} \frac{\partial T_a}{\partial t} dz \quad (5)$$

$$S_\lambda = \lambda \int_0^{z_r} \frac{\partial \rho_v}{\partial t} dz \quad (6)$$

where z_r is the height of the net radiation measurement (20 m). Air temperature (T_a) and humidity were measured with a temperature and relative humidity probe (HMP45C, Vaisala, Finland) at four heights (2, 3, 10 and 20 m). ρ_v was determined from HMP45C measurements of relative humidity and air temperature.

In calculating λE, the latent heat of vaporization λ_v (kJ kg^{-1}) or latent of sublimation λ_s (kJ kg^{-1}) was used for the half-hourly data, depending in the air temperature. If the air temperature T_a (°C) in the plant canopy (10 m) was positive, λ_v was calculated as (Fritschen and Gay, 1979)

$$\lambda_v = 2500.25 - 2.365 T_a \quad (7)$$

When T_a was zero or negative, λ_s was calculated as (Fleagle and Businger, 1980; Andreas, 2005)

$$\lambda_s = 2834.1 - 0.149 T_a \quad (8)$$

Supporting measurements

Parallel to the energy balance measurements, other supporting meteorological and soil measurements made at our site included photosynthetically active radiation (at the height of 19.20 m; LI190SB, LI-COR Inc.), precipitation (52 202 electrically heated rain/snow gage, RM Young, USA), soil temperature (109, Campbell Inc., USA) and volumetric water content (CS616, Campbell Scientific Inc.) profile (at 0.05, 0.1, 0.2, 0.4, 0.8 and 1.2 m below the soil surface), and snow depth (SR50, Campbell Scientific Inc.). The meteorological data were sampled every 1 s by data logger (CR23XTD, Campbell Scientific Inc.), and 30-min mean values were stored.

Measurements of tree height and DBH (1.37 m) were conducted during the experiment period. Leaf area index (m^2 m^{-2}) was measured once every 2 weeks using a plant canopy analyser (LI2000, LI-COR Inc.), adjusted for clumping index measured using the TRAC instrument (Third Wave Engineering, Ottawa, Canada).

Data processes, gap filling and energy balance closure

The half-hour sensible (H) and latent (λE) heat fluxes were calculated by EDIRE software (Clement, 1999) following the standard protocols including coordinate rotation, block averaging, despiking and air density correction (Webb *et al.*, 1980; Lee *et al.*, 2004). In addition, a friction velocity (u_*) filter was used to reject night-time fluxes when turbulence was low ($u_* < 0.15$ m s^{-1}: see details in Appendix B; Brown *et al.*, 2010, 2012). Approximately 20% of the night-time data was replaced as a result of low u_* conditions. The ratio of acceptable half-hourly H and λE measurements to the total data was 65%. Data gaps (no more than a few hours) were filled using linear interpolation. Larger gaps in flux data were replaced by average values calculated using the lookup table method (Falge *et al.*, 2001). Also, the uncertainties in the gap-filled annual evapotranspiration by using different u_* threshold values were estimated (Appendix B).

Energy balance closure is a requirement of the first law of thermodynamics, but lack of closure is a common feature for EC measurements, particularly at forested sites (Wilson *et al*., 2002b). Table I gives the results of energy balance closure determined by the linear regression method, using the sum of turbulent fluxes ($\lambda E + H$) relative to the available energy ($R_n - G - S$), for 30 min and daily total fluxes. We achieved energy balance closure of 0.81 ($H + \lambda E = 0.81$ ($R_n - G - S$) + 3.48, $r^2 = 0.83$) over the whole study period based on 30-min averages of the fluxes, and the closure status was higher in the growing seasons than that in the non-growing seasons (Table I). Closure increased to 0.94 when using the daily accumulated values instead of 30-min data. For FLUXNET sites, the slope values reported by Wilson *et al*. (2002b) range 0.53–0.99 with a mean of 0.79 ± 0.01, and the intercept values range -32.9–$36.9\ \mathrm{W\ m^{-2}}$ with a mean of $3.7 \pm 2.0\ \mathrm{W\ m^{-2}}$. Compared with these ranges, the energy balance closure statistics at our site were reasonable. Thus, the EC system provided consistent measurements of the atmosphere/surface exchanges of energy and mass.

Calculation of diagnostic parameters

Canopy surface conductance (g_c; $\mathrm{m\ s^{-1}}$) was calculated using the inverted form of the Penman–Monteith equation (Monteith and Unsworth, 1990):

$$\frac{1}{g_c} = \frac{\rho C_p}{\gamma \lambda E} D + \frac{1}{g_a}\left(\frac{\Delta}{\gamma}\frac{H}{\lambda E} - 1\right) \tag{9}$$

where D is the vapour pressure deficit (kPa), γ is the psychrometric constant ($\mathrm{kPa\ K^{-1}}$), Δ is the slope of relation between saturation vapour pressure and air temperature ($\mathrm{kPa\ K^{-1}}$), and g_a is aerodynamic conductance of the air layer between the canopy and the flux measurement height ($\mathrm{m\ s^{-1}}$), calculated assuming neutral stability as follows (Monteith and Unsworth, 1990):

$$\frac{1}{g_a} = \frac{u}{u_*^2} + 6.2 u_*^{-0.67} \tag{10}$$

Table I. Characteristics of energy balance ($\lambda E + H$) versus ($R_n - G - S$) using half-hourly and daily sum data values at the Qinghai–Tibet Plateau site

Data set	n	Slope	Intercept	R^2
30-min period				
All available data	14 938	0.81	3.48	0.83
Non-growing seasons (Nov.–Apr.)	7628	0.70	3.02	0.82
Growing seasons (May–Oct.)	7310	0.87	3.89	0.84
Daily mean				
All available data	319	0.94	−0.33	0.85
Non-growing seasons (Nov.–Apr.)	183	0.84	−0.01	0.80
Growing seasons (May–Oct.)	136	0.94	0.14	0.83

where u is the mean horizontal wind speed ($\mathrm{m\ s^{-1}}$) and u_* is the friction velocity obtained from EC measurement ($\mathrm{m\ s^{-1}}$). The decoupling coefficient (Ω) was obtained by the equation (Jarvis and McNaughton, 1986).

$$\Omega = \frac{\Delta + \gamma}{\Delta + \gamma(1 + g_a/g_c)} \tag{11}$$

To characterize the energy partitioning by the forest, we examined the variations of two derived variables, the evaporative fraction (Λ; Barr *et al*., 2001) and the Priestley–Taylor coefficient (α; Priestley and Taylor, 1972):

$$\Lambda = \frac{\lambda E}{\lambda E + H} \tag{12}$$

$$\alpha = \frac{\Delta + \gamma}{\gamma}\frac{\lambda E}{\lambda E + H} \tag{13}$$

The use of $\lambda E + H$ as the available energy flux in these two equations avoids the energy balance closure issue (Barr *et al*., 2001).

RESULTS AND DISCUSSION

Meteorological and biological conditions

Figure 1 shows the annual variations in meteorological and biological variables. Photosynthetically active radiation reached its maximum value in mid-June ($737\ \mu\mathrm{mol\ m^{-2}\ s^{-1}}$ on 12 June) and showed great day-to-day fluctuations during spring and summer periods due to frequent cloudy conditions, which are a common phenomenon on the QTP. The lowest air temperature (T_a) during winter was −20.5 °C (14 January) and the highest T_a was 19.2 °C (9 August). Mean annual T_a was 0.9 °C, and mean T_a in winter (DJF) and summer (JJA) was -10.9 and 12.5 °C, respectively. The vapour pressure deficit (D) was the highest in August, reaching 0.6 kPa (9 August). The mean annual D was 0.34 kPa, and mean D in winter and summer was 0.15 and 0.60 kPa, respectively. The variation in soil temperature (T_s) at different depths showed the gradual thawing of frozen soil, and the thaw dates at each depth were 19 April (5 cm), 6 May (10 cm), 23 May (20 cm), 21 June (40 cm), and 11 August (80 cm). From 20–27 October, these layers almost simultaneously began to freeze. The depth of the active layer was about 90 cm; 120 cm depth was within permafrost with its temperature below zero year-round. The variation in soil water content (θ_v) in depths from 0–20 cm were strongly dependent on the precipitation pattern. Annual precipitation was 428 mm, of which 60% falls in summer time. Leaf area index began to increase rapidly from late March ($<1.5\ \mathrm{m^2\ m^{-2}}$) and reached a maximum of $3.9\ \mathrm{m^2\ m^{-2}}$ in mid-July and then decreased slowly.

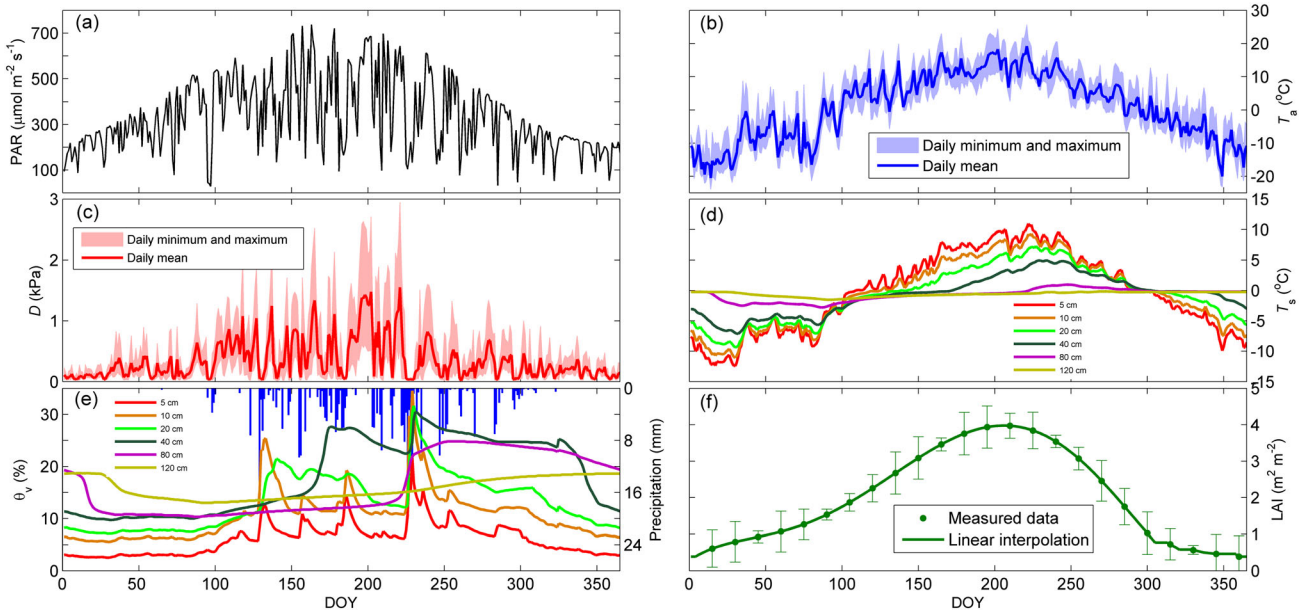

Figure 1. The annual course of the meteorological and biological conditions at the Qinghai spruce forest in 2011. (a) Daily (24-h) mean photosynthetically active radiation at height of 20 m, (b) air temperature at the height of 10 m in the plant canopy, (c) vapour pressure deficit (D) at the height of 10 m, (d) soil temperature, (e) volumetric soil water content (θ_v) and precipitation (bar blue) and (f) leaf area index. Air temperature (b) and vapour pressure deficit (c) are presented with daily average, maximum and minimum data, and precipitation is shown as daily accumulated values. Other data are 30-min average values

The radiation is shown in Figure 2. Daily-mean incoming shortwave radiation (S_d) showed significant seasonal and day-to-day variation, ranging from less than 5 W m^{-2} (28 October) to above 400 W m^{-2} (6 June). The difference between outgoing (L_u) and incoming (L_d) long wave was small on cloudy days and large on sunny days, ranging from less than 5 W m^{-2}–142 W m^{-2}. Daily mean albedo (the ratio of daily sums of reflected and incoming short-wave radiation) values were typically between 0.15 and 0.6, with a mean value of about 0.16 in summer and 0.46 in winter. The high value of albedo may be attributed to the snow cover on the plant canopy. Daily mean net radiation (R_n) closely followed the pattern of S_d, ranging from −10 W m^{-2} in winter (18 December) to 291 W m^{-2} in summer (27 July).

Diurnal patterns in energy balance components on typical clear days

Because of the distinct differences shown in the energy partitioning pattern, the year was divided into four periods: (1) the soil-frozen period (those days when the daily mean soil temperature at 5 cm was equal to or below 0 °C; Day of Year (DOY) 300–105); (2) the pre-growing period (with the daily mean soil temperature at 5 cm less than 5 °C and greater than 0 °C; DOY 106–145); (3) growth period (with the daily mean soil temperature at 5 cm was greater than 5 °C; DOY 146–258); and (4) the

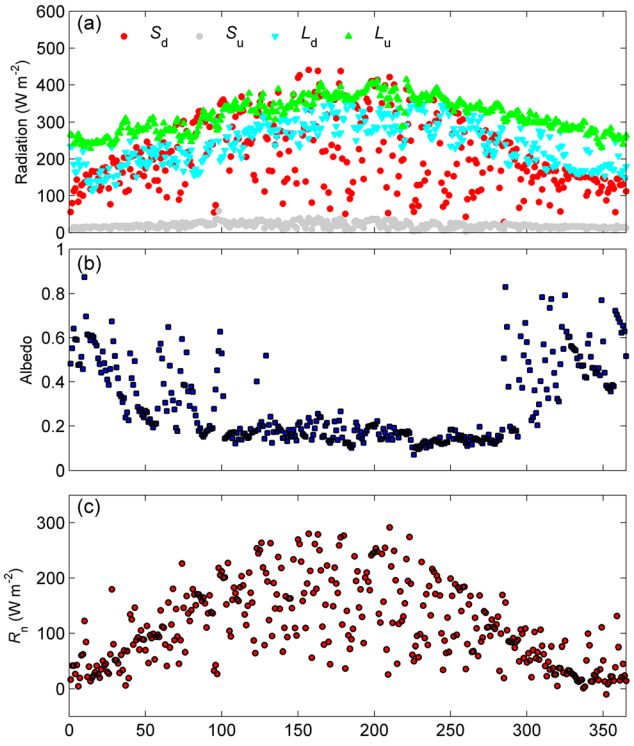

Figure 2. Seasonal variations in the daily (24-h) mean values of (a) incoming and reflected short-wave radiation (S_d, S_u), and incoming and outgoing long-wave radiation (L_d, L_u) at the 20 m; (b) Albedo of the forest canopy and (c) net radiation at the forest canopy

senescence period (with the daily mean soil temperature at 5 cm was less than 5 °C and greater than 0 °C; DOY 259–299). The different energy balance components and the diagnostic parameters were distinct for each of the four periods (Table II).

Figure 3 shows the diurnal variation in the ensemble means of different energy balance components on clear days during each period at this site. The daily period of positive R_n was considerably longer during the pre-growing and growth periods (on average between 8:00 and 20:00 h; Figure 3(b) and (c)) compared with the soil-frozen and senescence periods (on average between 9:00 and 18:00 h; Figure 3(a) and (d)). The daily highest values of R_n during each period were recorded during midday hours (about between 12:00 and 14:00 h), and were 540, 740, 800 and 600 W m^{-2} for the soil-frozen, pre-growing, growth and senescence periods, respectively. The diurnal behaviours of S were characterized by positive peaks around sunrise and negative peaks around sunset during each period. The highest half-hourly value of S was observed at the growth period (24 W m^{-2} at 9:00 h), whereas the lowest value was during the soil-frozen period (-10 m^{-2} at 19:00 h). The amplitude of the diurnal cycle of G was smaller than that of S during the soil-frozen and senescence periods and was comparable during the pre-growth and growth periods with its peaks between 15:00 and 17:00 h. Throughout the year, H was the dominant turbulent flux (Figure 3). The diurnal variations of H closely followed the pattern of R_n and the peak value occurring around the noon. In contrast, morning–afternoon asymmetry was observed in λE, which was usually larger in the morning than in the afternoon and slightly depressed at noon (Figure 3(c)). Earlier studies also showed that the stomata on the leaf surface of the alpine plants living on the QTP were partially closed under high solar radiation at noon to prevent excessive water loss (Cui *et al.*, 2003; Fu *et al.*, 2006). The average diurnal maximum value of H was observed at the pre-growing period (560 W m^{-2} at 12:00 h; Figure 3(b)), whereas the average daytime peak value of λE was during the growth period (259 W m^{-2} at 10:00 h; Figure 3(c)).

The daytime consumption of available energy ($=R_n - G - S$) for H and λE differed significantly over the sub-alpine forest ecosystem compared with the alpine grassland ecosystems in the QTP, where the summertime λE is generally greater than H (Gu *et al.*, 2005; Yao *et al.*, 2011). The different energy consumption patterns for forest and grassland located in the same climate zone should be attributed to the differences in their physiological (rooting depth, canopy

Table II. Daily means of the radiation, energy balance components and major biometeorological factors

	Whole year	Soil-frozen period (DOY 300–105)	Pre-growth period (DOY 106–145)	Growth period (DOY 146–258)	Senescence period (DOY 259–299)
T_a (°C)	0.94	−7.61	6.78	12.1	3.31
T_{s5} (°C)	−0.29	−6.16	2.11	7.86	2.27
θ_v (%)	6.10	3.54	7.70	9.09	7.81
D (kPa)	0.34	0.19	0.49	0.56	0.25
Precipitation (mm) (sum.)	428	14.4	60.9	303.4	49.3
LAI (m^2 m^{-2})	2.01	0.89	2.67	3.69	2.02
R_n (W m^{-2})	114.58	74.54	173.61	159.72	101.85
S_d (W m^{-2})	209.49	174.77	265.05	248.85	189.81
S_u (W m^{-2})	19.56	17.59	24.54	21.18	17.01
L_d (W m^{-2})	244.21	195.60	278.94	302.08	258.10
L_u (W m^{-2})	319.44	280.09	346.06	370.37	328.70
λE (W m^{-2})	32.52	6.13	55.21	68.98	28.70
H (W m^{-2})	71.06	57.18	104.17	81.48	63.08
G (W m^{-2})	0.23	−6.13	7.29	7.75	0.35
S (W m^{-2})	0	0	0.08	−0.02	−0.08
$\lambda E/R_n$	0.25	0.09	0.33	0.48	0.29
H/R_n	0.72	0.91	0.60	0.47	0.63
Λ	0.28	0.11	0.35	0.52	0.34
α	0.26	0.13	0.35	0.51	0.35
g_a (mm s^{-1})	350.2	316.1	436.5	392.5	376.7
g_c (mm s^{-1})	2.90	1.25	4.69	5.67	4.65
Ω	0.03	0.01	0.04	0.06	0.04

T_a, mean daily air temperature; T_{s5}, mean daily soil temperature at 5 cm depth; θ_v, mean daily soil volumetric water content from 0–20 cm depth; D, mean daily vapour pressure deficit; LAI, leaf area index; R_n, mean daily net radiation; S_d , mean daily incoming short-wave radiation; S_u , mean daily reflected short-wave radiation; L_d , mean daily incoming long-wave radiation; L_u , mean daily outgoing long-wave radiation; λE, mean daily latent heat flux; H, mean daily sensible heat flux; G, mean daily soil heat flux; S, mean daily heat storage; Λ, mean midday evaporative fraction; α, mean midday Priestley–Taylor coefficient; g_a, mean midday aerodynamic conductance; g_c, mean midday canopy surface conductance; Ω, mean midday decoupling factor. Midday was defined as 10:00 h through 16:00 h Beijing Standard Time (BST).

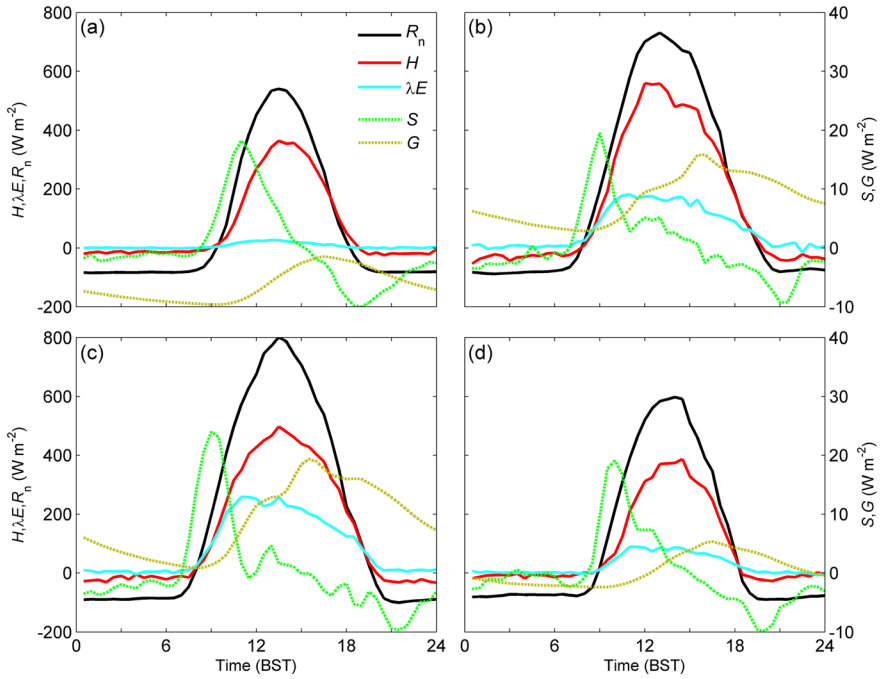

Figure 3. Averaged diurnal variations in net radiation flux (R_n), latent heat flux (λE), sensible heat flux (H), soil heat flux (G) and storage heat flux (S) for different periods: (a) soil-frozen period from DOY 300–108; (b) pre-growth period from DOY 109–161; (c) growth period from DOY 162–258 and (d) senescence period from DOY 259–299) at our site. Only data collected on clear days are presented. Beijing Standard Time (BST) is used here

structure, stomatal regulation) and eco-physical (surface albedo) parameters (Baldocchi *et al.*, 2004). In addition, the aerodynamic conductance (g_a) of grassland (generally $<30\,\mathrm{mm\,s^{-1}}$; Kelliher *et al.*, 1993) was much lower than that of the forest (more than $300\,\mathrm{mm\,s^{-1}}$; Table II). Thus, the efficient turbulent heat exchange of the forest relaxes the need for strong evaporative cooling when air temperature is high (Wicke and Bernhofer, 1996; Teuling *et al.*, 2010). Also, larger consumption for H than for λE, even at the peak growth stage, has been observed in many northern boreal forests (e.g. Jarvis *et al.*, 1997; McCaughey *et al.*, 1997; Kelliher *et al.*, 1997, 1998; Baldocchi *et al.*, 2000; Barr *et al.*, 2001; Ohta *et al.*, 2001; Matsumoto *et al.*, 2008) and some temperate coniferous forests (e.g. Restrepo and Arain, 2005; Kosugi *et al.*, 2007).

Seasonal variation in energy balance components

Seasonal variations of daily total values of R_n, H, λE and $G+S$ are shown in Figure 4. On a monthly basis, daily mean values of R_n for this ecosystem ranged from $53\,\mathrm{W\,m^{-2}}$ in winter to about $170\,\mathrm{W\,m^{-2}}$ in summer (Figure 4(a)). Daily mean values of S were an order of magnitude lower than G because at night the canopy essentially lost all of the heat it gained during daytime, and seasonal changes in heat storage flux ($G+S$) were dominated by G. There were a small yearly cycle in $G+S$ ranging from about -10–$10\,\mathrm{W\,m^{-2}}$, showing that the energy was stored in spring and summer and released in

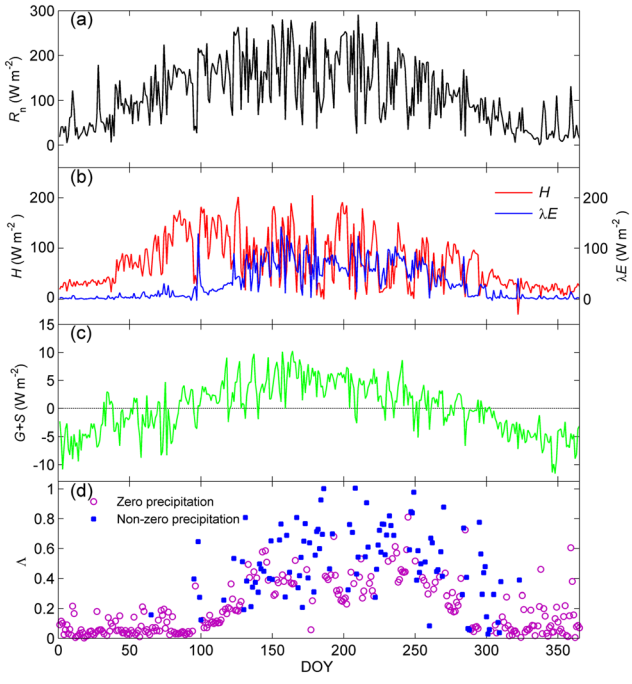

Figure 4. The annual course of daily average (a) net radiation R_n, (b) sensible heat H and latent heat λE, (c) soil heat flux plus canopy heat storage $G+S$ and (d) the evaporative fraction Λ

autumn and winter (Figure 4(c)). Overall, more than 95% of R_n was partitioned as H and λE, and the contributions of $G+S$ was very small. These results are consistent with

previous findings conducted at coniferous forests (e.g. Arain *et al*., 2003; Restrepo and Arian,). Recently, Nakai *et al*. (2013) reported that G played an important role in the energy balance for a boreal black spruce forest in interior Alaska, accounting for 14% of R_n. The site studied by Nakai *et al*. (2013) was characterized by low canopy density and high land-surface heterogeneity, so that the ground surface received a significant amount of direct solar radiation. Thus, the land surface condition and canopy characteristics may be important in determining the contribution of G.

From January to mid-April (DOY 1–105), R_n was small and mostly converted into H (Figure 4(b)). With the start of the growth of the vegetation and soil thawing on the QTP from late April to May (DOY 106–145), λE increased rapidly and H tended to decrease, even though R_n continued to increase. From late May to mid-September (DOY 146–258), the energy partitioning between λE and H was very similar and showed great day-to-day variations in response to changes in R_n and occurrences of precipitation (Figure 4(a) and (b)). It was noticed that moderate- to light-intensity storms (<5 mm) frequently occurred during the summer time on the QTP (Figure 1(e)), which increased the fraction of precipitation retained on plant surface. This intercepted precipitation subsequently evaporated rapidly, because there is no stomatal limitation (Baldocchi *et al*., 2004), resulting in high partition of R_n into λE. In contrast, H was the dominant turbulent flux on sunny days. When Λ was classified into zero precipitation and non-zero precipitation days, Λ of non-zero precipitation and zero precipitation during this period were 0.61 and 0.40, respectively (Figure 4(d)). In addition, observations showed that mean values of daily evapotranspiration flux during this period was 2.5 mm day^{-1}, with occasional values reaching up to 5 mm day^{-1}, mostly on days with or following rain (Figure 5(a)). During the vegetation senescence period (from mid-September to the end of October; DOY 259–299), λE started to decreased rapidly, and the energy was mostly consumed as H ($\Lambda < 0.4$) with the exception of days with or following rain (Figure 4(d)). After that, all energy flux components were small, and most of the available energy was partitioned as H.

The annual precipitation was 428 mm (rain/snow gauge measurement), and the precipitation (water equivalent) in winter was only 15 mm accounting for about 3.5% of annual precipitation. The annual evapotranspiration and sublimation (E, mm day^{-1}) is 417 ± 8 mm (Figure 5(b)), which indicated that about 98% of total annual precipitation returned to the atmosphere through evapotranspiration and sublimation. In addition, annual sublimation was estimated at 30 ± 2 mm year^{-1}, accounting for 7.9% of total annual evapotranspiration and sublimation. Thus, the sublimation in winter is not negligible in the annual

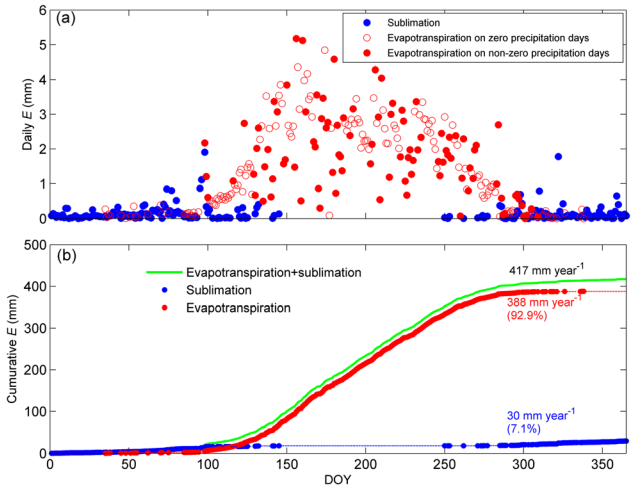

Figure 5. Seasonal variations in (a) daily evapotranspiration and sublimation (E, mm day^{-1}) and (b) cumulative evapotranspiration and sublimation (E, mm day^{-1}) calculated from half-hourly data

water balance of the sub-alpine/alpine ecosystems in QTP. Annual evapotranspiration at our site was estimated at 388 ± 9 mm (Figure 5(b)). This value was lower than that from temperate coniferous forest such as Douglas-fir forest in British Columbia, Canada (430 mm; Humphreys *et al*., 2003), ponderosa pine forest in Oregon, USA (400–430 mm; Anthoni *et al*.,1999) and pine plantation forest in southern Ontario, Canada (465 mm; Restrepo and Arain, 2005), but was larger than that from boreal forests such as black spruce forests in Saskatchewan, Canada (345–366 mm; Arain *et al*., 2003), in Fairbanks, Alaska (210 mm; Iwata *et al*., 2012) and in interior Alaska (189.0 mm; Nakai *et al*., 2013). Noticeably, the energy balance closure analysis suggests that there might be as much as a 19% underestimate of the annual total evapotranspiration. Thus, long-term observations and further studies are still needed to reveal the characteristics of the energy flux portioning and evapotranspiration in a sub-alpine spruce forest ecosystem.

Environmental and biological controls in evapotranspiration

To quantitatively estimate the relative importance of environmental and biological factors that control dry-canopy evapotranspiration, we investigated the seasonal behaviour of the mean midday values of α, g_c and Ω (Figure 6). The midday value was calculated using half-hourly meteorological and flux data from 10:00–16:00 h. Note that data with gap-filling and from days with or following rain were omitted for calculations and analyses.

The Priestley and Taylor (1972) α coefficient helps diagnose how biotic factors control daily forest evapotranspiration relative to the amount of available energy. An $\alpha < 1$ typifies a dry surface where limitations in water

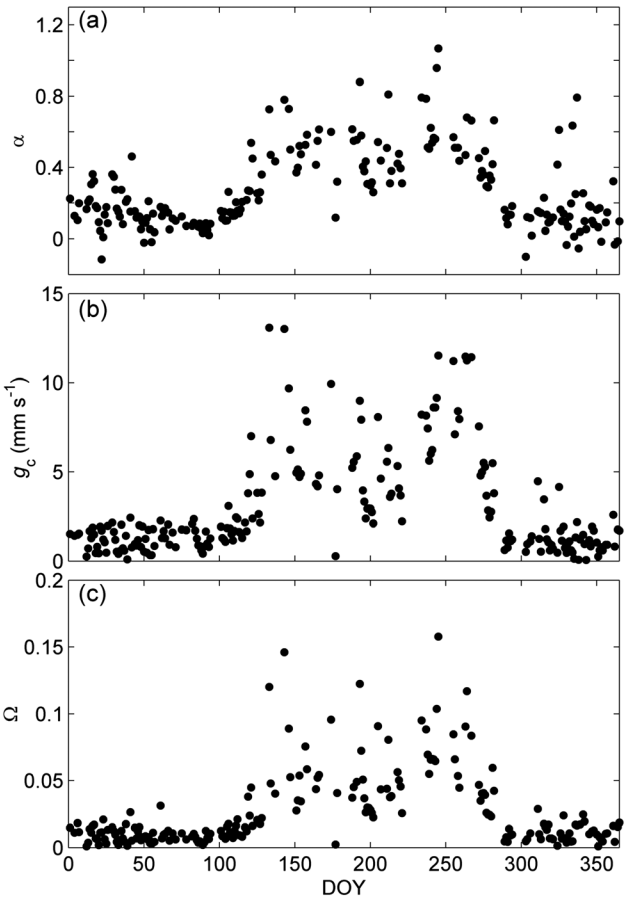

Figure 6. Seasonal variations in (a) Priestley–Taylor coefficient α, (b) bulk surface conductance g_c (mm s^{-1}) and (c) decoupling coefficient Ω. These values were calculated using half-hourly meteorological and flux data from 10:00–16:00 h (Beijing Standard Time)

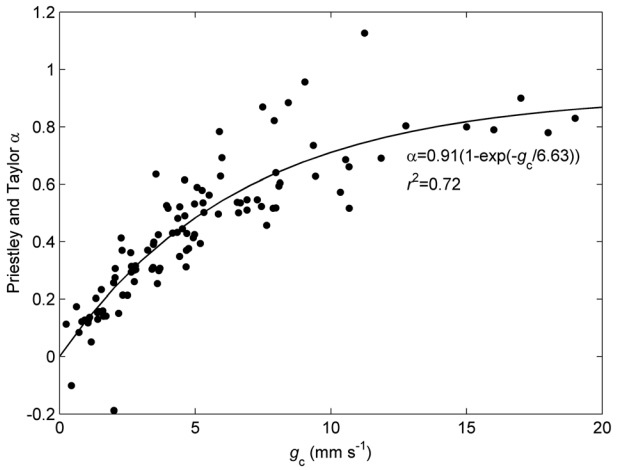

Figure 7. The relationship between mean midday (10:00–16:00 h on zero-precipitation days) Priestley–Taylor coefficient α and the bulk surface conductance g_c (mm s^{-1}). The non-line curve is fitted by the equation $\alpha = 0.91\left(1 - e^{-\frac{g_c}{6.63}}\right)$ ($r^2 = 0.72$)

supply is sufficient to reduce evapotranspiration, whereas $\alpha > 1$ typifies wet surfaces where the water supply is unrestricted, and available energy limits evaporation. The midday mean α for the sub-alpine forest was low during the soil-frozen period because frozen soil blocked the movement of soil moisture through the soil profile, and available energy exceed the available water supply in the cold winter. Even during the growth period, the midday mean α (0.51 ± 0.23) was also significantly below 1 (Figure 6(a) and Table II). The seasonal trend of g_c was similar to that of α (Figure 6(b)). The relationship between α and g_c showed that α was relatively insensitive to changes in g_c for conductance larger than 20 mm s^{-1} (Figure 7), which is consistent with the predictions by McNaughton and Spriggs (1989) using a mixed-layer model. The asymptotic value of α (0.91; Figure 7) was significant lower than the universal 1.1–1.4 range given regardless of surface wetness (Monteith, 1995), indicating that dry surface conditions dominate at this site. In addition, a strong inverse relationship between g_c and D was observed in this sub-alpine forest ecosystem (Figure.8). The low values of g_c and α on warm summer days (i.e. DOY195-221; Figure 6(a) and (b)), when D was at its highest values (Figure 1(c)), may likely a consequence of this relationship. This finding was similar to that of Brown *et al.* (2013) who reported that α values obtained at high soil water content were low when D was high at two lodgepole pine stands in the northern interior of British Columbia.

Small values of g_c and large values of g_a resulted in a very small Ω throughout the year. The mean value of Ω during the growth period was only 0.06 (Table II and Figure 6(b) and (c)), indicating that evapotranspiration from this sub-alpine forest was strongly coupled to the

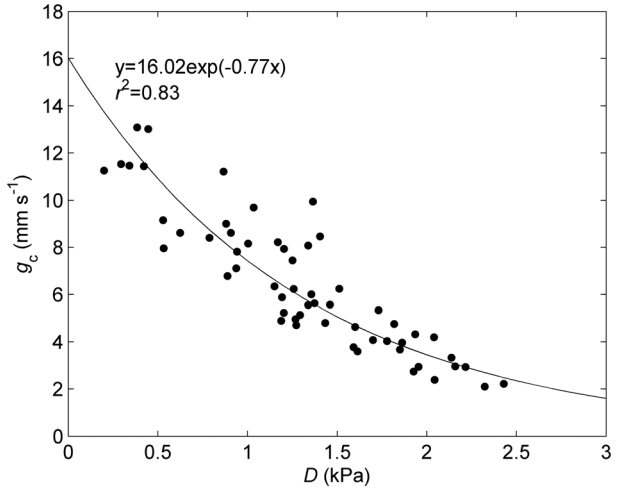

Figure 8. The relationship between mean midday (10:00–16:00 h on zero-precipitation days) bulk surface conductance g_c (mm s^{-1}) and vapour pressure deficit (D; kPa). The non-line curve is fitted by the equation $g_c = 16.02e^{-0.77D}$ ($r^2 = 0.83$)

atmosphere. The low values of α and Ω indicate that evapotranspiration is conservative and a large proportion of the available energy flux is in the form of H, which can result in a deep ABL with considerable entrainment of dry air from above the capping inversion, and further reduces g_c through positive feedback processes (McNaughton and Spriggs, 1989). Previous studies have indicated that the height of the ABL on the QTP can reach 2–3 km and is two times higher than that on the plain (Xu *et al*., 2002; Chen *et al*., 2013). Therefore, the sub-alpine forest ecosystems may play an important role in the development of the regional ABL over the QTP.

These results have wider implications for understanding the effects of climate changes on high mountain plants. Under warm conditions, H and canopy temperature were enhanced because of the inverse relationship between g_c and D. To prevent heat injury, plants are expected to migrate upwards in elevation towards colder climes. There is much evidence of elevational shifts of distributions of mountain plants to recent warming (e.g. Parmesan, 1996; Parmesan and Yohe, 2003; Walther *et al*., 2005; Thomas, 2010; Chen *et al*., 2011). Thus, predictive modelling of the climate effects on mountain plants should take into account the characteristics of energy flux partitioning in mountain plant ecosystems in future studies.

CONCLUSIONS

We measured EC energy fluxes over a permafrost Qinghai spruce (*P. crassifolia*) forest on the QTP in 2011 and examined the characteristics of the energy flux partitioning and evapotranspiration from this sub-alpine forest. Several conclusions can be drawn from this study:

1. In this sub-alpine forest ecosystem, the partitioning of available energy was mainly in the form of H, even in summer. However, the rainfall events had a significant influence on the energy flux partitioning and evapotranspiration. The mean value of Λ during the growth period on zero precipitation days and non-zero precipitation days was 0.40 and 0.61, respectively.
2. The mean daily evapotranspiration in the spring, summer and autumn was 1.05, 2.56 and 0.82 mm day^{-1}, respectively. In winter, the mean evaporation was 0.11 mm day^{-1}, mostly as a result of sublimation. The annual evapotranspiration and sublimation was 417 ± 8 mm year^{-1}, which was very comparable with the annual precipitation (428 ± 9 mm), with 7.1% (30 ± 2 mm year^{-1}) attributed to sublimation.
3. The values of the α and Ω were low during most of the growing season, indicating dry soil conditions and conservative water loss in this sub-alpine forest.

ACKNOWLEDGEMENTS

The authors would like to thank Prof. Doerthe Tetzlaff (Associate Editor) for the valuable suggestions and continuous helps on an earlier draft of the manuscript. We also thank the three anonymous reviewers for their critical reviews and helpful comments. This research was supported by the Fundamental Research Funds for the Central Universities (Nos. lzujbky-2013-m02 and lzujbky-2013-k19), National Natural Science Foundation of China (No. 41001242) and New Century Excellent Talents in University of Chinese Ministry of Education (No. NCET-11-0219).

REFERENCES

Andreas E. 2005. *Handbook of Physical Constants and Functions for Use in Atmospheric Boundary Layer Studies*. U.S. Army Cold Regions Research and Engineering Laboratory: Hanover, NH.

Anthoni PM, Law BE, Unsworth MH. 1999. Carbon and water vapor exchange of an open-canopied ponderosa pine ecosystem. *Agricultural and Forest Meteorology* **95**: 151–168.

Arain MA, Black TA, Barr AG, Griffis TJ, Morgenstern K, Nesic Z. 2003. Year-round observations of the energy and water vapour fluxes above a boreal black spruce forest. *Hydrologie Continentale* **17**: 3581–3600.

Baldocchi DD, Vogel CA. 1995. Energy and CO_2 flux densities above and below a temperate broad-leaved forest and a boreal pine forest. *Tree Physiology* **16**: 5–16.

Baldocchi DD, Vogel CA. 1996. Energy and CO_2 flux densities above and below a temperate broad-leaved forest and a boreal pine forest. *Tree Physiology* **16**: 5–16.

Baldocchi D, Kelliher FM, Black TA, Jarvis P. 2000. Climate and vegetation controls on boreal zone energy exchange. *Global Change Biology* **6**(Suppl. 1): 69–83.

Baldocchi D, Falge E, Gu L, Olson R, Hollinger D, Running S, Anthoni P, Bernhofer C, Davis K, Evans R, Fuentes J, Goldstein A, Katul G, Law B, Lee X, Maihi Y, Meyers T, Munger W, Oechel W, Paw UKT, Pilegaard K, Schmid HP, Valentini R, Verma S, Vesala T, Wilson K, Wofsy S. 2001. FLUXNET: a new tool to study the temporal and spatial variability of ecosystem-scale carbon dioxide, water vapor, and energy flux densities. *Bulletin of the American Meteorological Society* **82**: 2415–2434.

Baldocchi DD, Xu LK, Kiang N. 2004. How plant functional-type, weather, seasonal drought, and soil physical properties alter water and energy fluxes of an oak-grass savanna and an annual grassland. *Agricultural and Forest Meteorology* **123**: 13–39.

Barr AG, Betts AK, Black TA, McCaughey JH, Smith CD. 2001. Intercomparison of BOREAS northern and southern study area surface fluxes in 1994. *Journal of Geophysical Research* **106**(D24): 33543–33550.

Betts RA. 2000. Offset of the potential carbon sink from boreal afforestation by decreases in surface albedo. *Nature* **408**: 187–190.

Blanken PD, Black TA, Yang PC, Neumann HH, Nesic Z, Staebler R, den Hartog G, Novak MD, Lee X. 1997. Energy balance and canopy conductance of a boreal aspen forest: partitioning overstory and understory components. *Journal of Geophysical Research* **102**: 28915–28917.

Bourque CPA, Mir MA. 2012. Seasonal snow cover in the Qilian Mountains of Northwest China: its dependence on oasis seasonal evolution and lowland production of water vapour. *Journal of Hydrology* **454**: 141–151.

Brown MG, Black TA, Nesic Z, Foord VN, Spittlehouse DL, Fredeen AL, Grant NJ, Burton PJ, Trofymow JA. 2010. Impact of mountain pine beetle on the net ecosystem production of lodgepole pine stands in British Columbia. *Agricultural and Forest Meteorology* **150**: 254–264.

Brown MG, Black TA, Nesic Z, Fredeen AL, Foord VN, Spittlehouse DL, Bowler R, Burton PJ, Trofymow JA, Grant NJ, Lessard D. 2012. The carbon balance of two lodgepole pine stands recovering from mountain

pine beetle attack in British Columbia. *Agricultural and Forest Meteorology* **153**: 82–93.

Brown MG, Black TA, Nesic Z, Foord VN, Spittlehouse DL, Fredeen AL, Bowler R, Grant NJ, Burton PJ, Trofymow JA, Lessard D, Meyer G. 2013. Evapotranspiration and canopy characteristics of two lodgepole pine stands following mountain pine beetle attack. *Hydrologie Continentale*. DOI: 10.1002/hyp.9870.

Brubaker KL, Entekhabi D. 1996. Analysis of feedback mechanisms in land–atmosphere interaction. *Water Resources Research* **32**(5): 1343–1357.

Chen IC, Hill JK, Ohlemüller R, Roy DB, Thomas CD. 2011. Rapid range shifts of species associated with high levels of climate warming. *Science* **333**: 1024–1025.

Chen X, Anel JA, Su Z, de la Torre L, Kelder H, van Peet J, Ma Y. 2013. The deep atmospheric boundary layer and its significance to the stratosphere and troposphere exchange over the Tibetan Plateau. *PLoS ONE* **8**(2): e56909. DOI: 10.1371/journal.pone.0056909.

Clement R. 1999. EdiRe Data Software. Version 1.4.3.1101, University of Edinburgh: UK; http://www.geos.ed.ac.uk/abs/research/micromet/EdiRe.

Cui XY, Tang YH, Gu S, Nishimura S, Shi SB, Zhao XQ. 2003. Photosynthetic depression in relation to plant architecture in two alpine herbaceous species. *Environmental and Experimental Botany* **50**: 125–135.

Falge E, Baldocchi D, Olson R, Anthoni P, Aubinet M, Bernhofer Ch, Burba G, Ceulemans R, Clement R, Dolman H, Granier A, Gross P, Grunwald T, Hollinger D, Jenson N-O, Katul G, Keronen P, Kowalski A, Lai CT, Law B, Meyers T, Moncrieff J, Moors EJ, Munger W, Pilegaard K, Rannik U, Rebmann C, Sukyer A, Tenhunen J, Tu K, Verma S, Vesala T, Wilson K, Wofsy S. 2001. Gap filling strategies for defensible annual sums of net ecosystem exchange. *Agricultural and Forest Meteorology* **107**: 43–69.

Fisher RA, Williams M, de Lourdes Ruivo M, de Costa AL, Meir P. 2008. Evaluating climatic and soil water controls on evapotranspiration at two Amazonian rainforest sites. *Agricultural and Forest Meteorology* **148**(6–7): 850–861.

Fleagle R, Businger J. 1980. *An Introduction to Atmospheric Physics*, 2nd edn. Academic Press: New York.

Fritschen L, Gay L. 1979. *Environmental Instrumentation*. Springer-Verlag: New York.

Fu YL, Yu GR, Sun XM, Li YN, Wen XF, Zhang LM, Li ZY, Zhao L, Hao YB. 2006. Depression of net ecosystem CO_2 exchange in semi-arid Leymus chinensis steppe and alpine shrub. *Agricultural and Forest Meteorology* **137**: 234–244.

Giambelluca TW, Martin RE, Asner GP, Huang M, Mudd RG, Nullet MA, DeLay JK, Foote D. 2009. Evapotranspiration and energy balance of native wet montane cloud forest in Hawai'i. *Agricultural and Forest Meteorology* **149**(2): 230–243.

Gu S, Tang YH, Cui XY, Kato T, Du MY, Li YN, Zhao XQ. 2005. Energy exchange between the atmosphere and a meadow ecosystem on the Qinghai–Tibetan Plateau. *Agricultural and Forest Meteorology* **129**: 175–185.

Gu L, Meyers T, Pallardy SG, Hanson PJ, Yang B, Heuer M, Hosman KP, Riggs JS, Sluss D, Wullschleger SD. 2006. Direct and indirect effects of atmospheric conditions and soil moisture on surface energy partitioning revealed by a prolonged drought at a temperate forest site. *Journal of Geophysical Research* **111**: D16102. DOI: 10.1029/2006JD007161.

Hsieh C, Katul G, Chi T. 2000. An approximate analytical model for footprint estimation of scalar fluxes in thermally stratified atmospheric flows. *Advances in Water Resources* **23**: 765–772.

Humphreys ER, Black TA, Ethier GJ, Drewitt GB, Spittlehouse DL, Jork EM, Nesic Z, Livingston NJ. 2003. Annual and seasonal variability of sensible and latent heat fluxes above a coastal Douglas-fir forest, British Columbia, *Canadian Society of Agricultural and Forest Meteorology* **115**: 109–125.

IPCC (Intergovernmental Panel on Climate Change). 2007. Climate change 2007: impacts, adaptation and vulnerability. In *Contribution of Working Group II to the Fourth Assessment Report of the Intergovernmental Panel on Climate Change*, Parry M, *et al*. (eds). Cambridge University Press: Cambridge, United Kingdom; 470–506.

Iwata H, Harazono Y, Ueyama M. 2012. The role of permafrost in water exchange of a black spruce forest in interior Alaska. *Agricultural and Forest Meteorology* **161**: 107–115.

Jarvis PG, McNaughton KG. 1986. Stomatal control of transpiration-scaling up from leaf to region. *Advances in Ecological Research* **15**: 1–49.

Jarvis PG, Massheder JM, Hale SE, Moncrieff JB, Rayment M, Scott SL. 1997. Seasonal variation of carbon dioxide, water vapor, and energy exchange of a boreal black spruce forest. *Journal of Geophysical Research* **102**: 28953–28966.

Jassal RS, Black TA, Spittlehouse DL, Brummer C, Nesic Z. 2009. Evapotranspiration and water use efficiency in different-aged Pacific Northwest Douglas-fir stands. *Agricultural and Forest Meteorology* **149**(6-7): 1168–1178.

Kelliher FM, Leuning R, Schulze ED. 1993. Evaporation and canopy characteristics of coniferous forests and grasslands. *Oecologia* **95**: 153–163.

Kelliher FM, Hollinger DY, Schulze ED, Vygodskaya NN, Byers JN, Hunt JE, McSeveny TM, Milukova I, Sogatchev A, Varlargin A, Ziegler W. Arneth A, Bauer G. 1997. Evaporation from an eastern Siberian larch forest. *Agricultural and Forest Meteorology* **85**: 135–147.

Kelliher FM, Lloyd J, Arneth A, Byers JN, McSeveny TM, Milukova I, Grigoriev S, Panfyorov M, Sogatchev A, Varlargin A, Ziegler W. Bauer G, Schulze ED. 1998. Evaporation from a central Siberian pine forest. *Journal of Hydrology* **205**: 279–296.

Kochendorfer J, Castillo EG, Haas E, Oechel WC, Paw UKT. 2011. Net ecosystem exchange, evapotranspiration and canopy conductance in a riparian forest. *Agricultural and Forest Meteorology* **151**(5): 544–553.

Kosugi Y, Takanashi S, Tanaka H, Ohkubo S, Tani M, Yano M, Katayama T. 2007. Evapotranspiration over a Japanese cypress forest. I. Eddy covariance fluxes and surface conductance characteristics for 3 years. *Journal of Hydrology* **337**: 269–283.

Kumagai TO, Saitoh TM, Sato Y, Takahashi H, Manfroi OJ, Morooka T, Kuraji K, Suzuki M, Yasunari T, Komatsu H. 2005. Annual water balance and seasonality of evapotranspiration in a Bornean tropical rainforest. *Agricultural and Forest Meteorology* **128**(1-2): 81–92.

Kume T, Tanaka N, Kuraji K, Komatsu H, Yoshifuji N, Saitoh TM, Suzuki M, Kumagai T. 2011. Ten-year evapotranspiration estimates in a Bornean tropical rainforest. *Agricultural and Forest Meteorology* **151**: 1183–1192.

Lee X, Massman WJ, Law BE. 2004. *Handbook of Micrometeorology: A Guide for Surface Flux Measurement and Analysis*. Kluwer Academic Publishers: Dordrecht, The Netherlands.

Li X, Li XW, Li ZY, Ma MG, Wang J, Xiao Q, Liu QH, Che T, Chen EX, Yan GJ, Hu ZY, Zhang LX, Chu RZ, Su PX, Liu QH, Liu SM, Wang JD, Niu Z, Chen Y, Jin R, Wang WZ, Xin ZZ, Ren HZ. 2009. Watershed allied telemetry experimental research. *Journal of Geophysical Research* **114**: D22103. DOI: 10.1029/2008JD011590.

LI-COR Inc. 2000. *LI-7500 CO_2/H_2O Analyzer Instruction Manual*. LI-COR Inc.: Lincoln, NE.

Liu XD, Chen BD. 2000. Climatic warming in the Tibetan Plateau during recent decades. *International Journal of Climatology* **20**(14): 1729–1742.

Liu XM, Liu XD, Che ZX, Zhang RS. 2010. Eco-hydrological functions of the moss layer in *Picea crassifolia* forest of Qilian Mountains. *Arid Land Geography* **33**(6): 962–967 (in Chinese with English abstract).

Matsumoto K, Ohta T, Nakai T, Kuwada T, Daikoku K, Iida S, Yabuki H, Kononov AV, van der Molen MK, Kodama Y, Maximov TC, Dolman AJ, Hattori S. 2008. Energy consumption and evapotranspiration at several boreal and temperate forests in the Far East. *Agricultural and Forest Meteorology* **148**: 1978–1989.

McCaughey JH, Lafleur PM, Joiner DW, Bartlett PA, Costello AM, Jelinski DE, Ryan MG. 1997. Magnitudes and seasonal patterns of energy, water, and carbon exchanges at a boreal young jack pine forest in the BOREAS northern study area. *Journal of Geophysical Research* **102**(D24): 28997–29007.

McCaughey JH, Pejam MR, Arain MA, Cameron DA. 2006. Carbon dioxide and energy fluxes from a boreal mixed-wood forest ecosystem in Ontario, Canada. *Agricultural and Forest Meteorology* **140**(1-4): 79–96.

McNaughton KG, Spriggs TW. 1989. An evaluation of the Priestley and Taylor equation and the complementary relationship using results from a mixed-layer model of the convective boundary layer. In *Estimation of Areal Evapotranspiration*, Black TA, Spittlehouse DL, Novak MD, Price DT (eds). IAHS Publication: Vancouver, Canada; 89–104.

Monteith JL, Unsworth MH. 1990. *Principles of Environmental Physics*, 2nd edn. Chapman & Hall: New York, USA.

Monteith JL. 1995. A reinterpretation of stomatal responses to humidity, *Plant, Cell and Environment* **18**: 357–364.

Nakai T, Kim Y, Busey RC, Suzuki R, Nagai S, Kobayashi H, Park H, Sugiura K, Ito A. 2013. Characteristics of evapotranspiration from a

permafrost black spruce forest in interior Alaska. Polar Science, Available from: http://dx.doi.org/10.1016/j.polar.2013.03.003.

Ohta T, Hiyama T, Tanaka H, Kuwada T, Maximov TC, Ohata T, Fukushima Y. 2001. Seasonal variation in the energy and water exchanges above and below a larch forest in eastern Siberia. *Hydrologie Continentale* **15**: 1459–1476.

Ohta T, Maximov TC, Dolman AJ, Nakai T, van der Molen MK, Kononov AV, Maximov AP, Hiyama T, Iijima Y, Moors EJ, Tanaka H, Toba T, Yabuki H. 2008. Interannual variation of water balance and summer evapotranspiration in an eastern Siberian larch forest over a 7-year period (1998–2006). *Agricultural and Forest Meteorology* **148**(12): 1941–1953.

Oliphant AJ, Grimmond CSB, Zutter HN, Schmid HP, Su H-B, Scott SL, Offerle B, Randolph JC, Ehman J. 2004. Heat storage and energy balance fluxes for a temperate deciduous woodland. *Agricultural and Forest Meteorology* **126**: 185–201.

Parmesan C. 1996. Climate and species' range. *Nature* **382**: 765–766.

Parmesan C, Yohe G. 2003. A globally coherent fingerprint of climate change impacts across natural systems. *Nature* **421**: 37–42.

Pejam MR, Arain MA, McCaughey JH. 2006. Energy and water vapour exchanges over a mixedwood boreal forest in Ontario, *Canadian hydrological processes* **20**(17): 3709–3724.

Priestley CHB, Taylor RJ. 1972. On the assessment of surface heat flux and evaporation using large-scale parameters. *Monthly Weather Review* **100**: 81–92.

Raupach MR. 1998. Influences of local feedbacks on land–air exchanges of energy and carbon. *Global Change Biology* **4**: 477–494.

Restrepo NC, Arain MA. 2005. Energy and water exchanges from a temperate pine plantation forest. *Hydrologie Continentale* **19**(1): 27–49.

Sánchez JM, Caselles V, Rubio EM. 2010. Analysis of the energy balance closure over a FLUXNET boreal forest in Finland. *Hydrology and Earth System Sciences* **14**(8): 1487–1497.

Tanaka N, Kume T, Yoshifuji N, Tanaka K, Takizawa H, Shiraki K, Tantasirin C, Tangtham N, Suzuki M. 2008. A review of evapotranspiration estimates from tropical forests in Thailand and adjacent regions. *Agricultural and Forest Meteorology* **148**(5): 807–819.

Teuling AJ, Seneviratne SI, Stöckli R, Reichstein M, Moors E, Ciais P, Luyssaert S, van den Hurk B, Ammann C, Bernhofer C, Dellwik E, Gianelle D, Gielen B, Grünwald T, Klumpp K, Montagnani L, Moureaux C, Wohlfahrt G. 2010. Contrasting response of European forest and grassland energy exchange to heatwaves. *Nature Geoscience* **3**: 722–727.

Thomas CD. 2010. Climate, climate change, and range boundaries. *Diversity and Distributions* **16**: 488–495.

Walther GR, Sascha1 B, Burga CA. 2005. Trends in the upward shift of alpine plants. *Journal of Vegetation Science* **16**: 541–548.

Webb EK, Pearman GI, Leuning R. 1980. Correction of flux measurements for density effects due to heat and water vapour transfer. *Quarterly Journal of the Royal Meteorological Society* **106**: 85–100.

Wicke W, Bernhofer C. 1996. Energy balance comparison of the Hartheim forest and an adjacent grassland site during the HartX experiment. *Theoretical and Applied Climatology* **53**: 49–58.

Wilson KB, Baldocchi DD. 2000. Seasonal and interannual variability of energy fluxes over a broadleaved temperature deciduous forest in North America. *Agricultural and Forest Meteorology* **100**: 1–18.

Wilson KB, Baldocchi DD, Aubinet M, Berbigier P, Bernhofer C, Dolman H, Falge E, Field C, Goldstein A, Granier A, Grelle A, Halldor T, Hollinger D, Katul G, Law BE, Lindroth A, Meyers T, Moncrieff J, Monson R, Oechel W, Tenhunen J, Valentini R, Verma S, Vesala T, Wofsy S. 2002a. Energy partitioning between latent and sensible heat flux during the warm season at FLUXNET sites. *Water Resources Research* **38**(12): 1294. DOI: 10.1029/2001WR000989.

Wilson KB, Goldstein A, Falge E. 2002b. Energy balance closure at FLUXNET sites. *Agricultural and Forest Meteorology* **113**: 223–243.

Wu JB, Guan DX, Han SJ, Shi TT, Jin CJ, Pei TF, Yu GR. 2007. Energy budget above a temperate mixed forest in northeastern China. *Hydrologie Continentale* **21**: 2425–2434.

Wu J, Jing Y, Guan D, Yang H, Niu L, Wang A, Yuan F, Jin C. 2012. Controls of evapotranspiration during the short dry season in a temperate mixed forest in Northeast China. *Ecohydrology*. DOI: 10.1002/eco.1299.

Xu X, Zhou M, Chen J, Bian L, Zhang G, Liu H, Li S, Zhang H, Zhao Y, Suolongduoji Wang J. 2002. A comprehensive physical pattern of land-air dynamic and thermal structure on the Qinghai-Xizang Plateau. *Science in China (Series D)* **45**(7): 577–594.

Yao JM, Zhao L, Gu LL, Qiao YP, Jiao KQ. 2011. The surface energy budget in the permafrost region of the Tibetan Plateau. *Atmospheric Research* **102**: 394–407.

Zheng D. 1996. The system of physico-geographical regions of the Qinghai-Xizang (Tibet) Plateau. *Science in China Series D* **39**: 410–417.

Zhu GF, Li ZZ, Su YH, Ma JZ, Zhang YY. 2007. Hydrogeochemical and isotope evidence of groundwater evolution and recharge in Minqin Basin, Northwest China. *Journal of Hydrology* **333**: 239–251.

Zhu GF, Su YH, Feng Q. 2008. The hydrochemical characteristics and evolution of groundwater and surface water in the Heihe River Basin, northwest china. *Hydrogeology Journal* **16**: 167–182.

